machines

MDPI

Article

MOPSO-Based Design Optimization for Armature Coils in High-Propulsive-Force Electrodynamic Vibrators

Xiaohong Fu [1,2], Minggang Zhu [1,*], Jianping Shen [3] and Zhigang Liu [1]

[1] College of Power and Energy Engineering, Harbin Engineering University, Harbin 150001, China; fu.xh@sndnt.com (X.F.)
[2] Dongling Technologies Co., Ltd., Suzhou 215163, China
[3] Shanghai Marine Diesel Engine Research Institute, Shanghai 201108, China; sjp2016@outlook.com
* Correspondence: zhuminggang@hrbeu.edu.cn

Abstract

Directly coupled electrodynamic vibrators are widely used in vibration testing due to their ability to generate large propulsive forces. However, increasing the propulsive force typically requires higher driving currents, which leads to significant electrical heat generation and thermal management challenges in the armature coil. To address this issue, this study proposes a multi-objective parameter optimization framework for the design of armature coils in high-propulsive-force electrodynamic vibration tables. Two optimization objectives are formulated based on electromagnetic and thermal considerations: minimization of electrical heat generation in the armature coil; and improvement in cooling capability, characterized by the ratio between the cooling water channel area and the conductive cross-sectional area. The key geometric parameters of the coil, including winding configuration and cross-sectional dimensions, are treated as design variables. The resulting multi-objective optimization problem is solved using a multi-objective particle swarm optimization (MOPSO) algorithm to obtain a set of Pareto-optimal solutions that balance the two competing thermal objectives. The present work focuses on the pre-design-stage optimization of the armature coil after the rated propulsive force and geometric envelope of the vibrator have been specified. A representative high-propulsive-force electrodynamic vibrator is analyzed as a case study. Finite element thermal simulations show that the selected Pareto-optimal design reduces the peak armature-coil temperature by approximately 9.7–36.6% compared with the other investigated coil configurations under the same propulsive force condition. The proposed method provides an efficient approach for the thermally constrained parameter design of high-power electrodynamic vibrator armature coils.

Keywords: electrodynamic vibrator; armature coil optimization; multi-objective optimization; particle swarm optimization (PSO); finite element analysis

Check for updates

Academic Editor: Parviz Famouri

Received: 15 April 2026
Revised: 9 June 2026
Accepted: 18 June 2026
Published: 20 June 2026

Copyright: © 2026 by the authors. Licensee MDPI, Basel, Switzerland. This article is an open access article distributed under the terms and conditions of the Creative Commons Attribution (CC BY) license.

1. Introduction

Vibration is unavoidable in mechanical systems, making vibration testing an indispensable procedure for evaluating structural reliability. This requirement led to the development of vibrators. Common vibrators can be classified into hydraulic vibrators and electrodynamic vibrators. Among them, directly coupled electrodynamic vibrators are widely used due to their larger maximal propulsive force. The basic structure of an electrodynamic vibrator with permanent magnet [1] is shown in Figure 1. The magnetic field created

by the permanent magnet is guided by the body and inner pole of the vibrator, forming an approximately uniform magnetic field in the air gap. The armature coil is subjected to alternating current and moves back and forth in a uniform magnetic field. With this principle, the vibrator generates the vibration of the shaker table in the vibration tests.

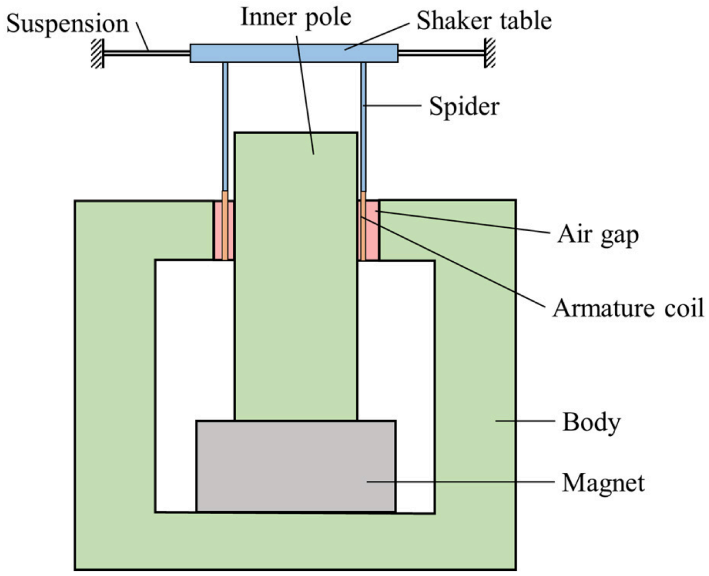


Figure 1. Main structure of electrodynamic vibrator.

In large-propulsive-force electrodynamic vibrators, electromagnets are typically employed instead of permanent magnets to generate a stronger magnetic field in the air gap. When an alternating current flows through the armature coil, the coil is subjected to alternating electromagnetic forces within the magnetic field, producing reciprocating motion. At present, electrodynamic vibrators have been widely applied to vibration testing of various structures in aerospace, aeronautics, civil engineering, and other fields [2–5].

With the increasing trend toward large-scale and high-precision mechanical structures, integrated testing of large structures becomes necessary, which further increases the demand for higher propulsive force. For electrodynamic vibrators, larger propulsive force not only implies larger dimensions, but also requires higher currents to generate greater electromagnetic forces [6]. However, higher current leads to increased heat generation in the electrical circuit, and excessive temperatures can significantly reduce the service life of certain circuit components and electrical connections. Therefore, during the design of vibrators, in addition to considering performance requirements such as size and propulsive force, it is also necessary to take the heat generation characteristics of the electrical system into account. To increase the current in the armature coil and thus improve vibrator propulsive force, multilayer winding structures could be adopted; however, the increase in design parameters further complicates the design process.

To improve design efficiency and provide reliable guidance for parameter selection, one effective approach is to reformulate the parameter design problem as a constrained optimization problem. The key is to exploit the characteristic performance of the mechanical system to construct appropriate objective functions. The optimal parameter values corresponding to favorable system performance can be obtained using these objective functions. In robot design, parameter optimization can enhance system performance [7]. In structural design, simulation techniques can automate the design process and improve efficiency [8]. In manufacturing, the optimization of process parameters improves economic performance, efficiency, and effectiveness [9]. Xu et al. optimized two design parameters of a three-degree-of-freedom parallel manipulator based on kine-

matic performance [10]. Khan and Angeles introduced the concepts of "homogeneous space" and "norm functions" in robot dimensional optimization [11]. Qiu et al. designed a bio-inspired origami jellyfish mechanism and achieved parameter optimization by maximizing the volume ratio and the range of slenderness ratios [12]. Zhakatayev et al. proposed a homotopy optimization method for identifying unknown parameters in implicit differential equations [13]. Sangalli et al. optimized the load distribution of ball screws, reducing non-uniformity and increasing stiffness, thereby extending service life by a factor of 17 [14]. Zhang et al. optimized the structural parameters of vertically aligned small-beam beetle elytron plates based on mechanical and thermal performance [15]. These studies demonstrate that, during the design stage, optimization methods can identify design schemes that yield favorable performance of the mechanical system and significantly improve design efficiency.

In the design optimization of mechanical systems, more than one optimization objective typically needs to be considered, and these objectives may constrain one another. Consequently, multi-objective optimization methods are required to solve such design optimization problems. The goal of multi-objective optimization is to determine the Pareto front set [16]. Lalwani et al. reviewed MOPSO applications in multiple fields and emphasized its ability to generate Pareto-optimal solution sets for problems with conflicting objectives [17]. This feature is suitable for the present armature-coil design problem, because reducing Joule heat generation and maintaining sufficient cooling-channel space cannot generally be achieved by the same extreme design. Among commonly used approaches, swarm-based techniques represent an important class of algorithms [18]. Standard Particle Swarm Optimization (PSO) was proposed based on the collective behavior of bird flocks or fish schools [19,20]. One of the main advantages of PSO lies in its simplicity, ease of implementation, small number of parameters, and minimal requirements for objective functions, which enable its application to a wide range of optimization problems [21,22]. Li et al. used multi-objective PSO (MOPSO) to optimize the design of wind turbine blades, reducing average noise pressure while satisfying strength and stiffness requirements and improving efficiency [23]. Zhang et al. utilized MOPSO to optimize measurement accuracy and noise suppression performance in vibration measurement, and applied it to the vibration measurement of scale-down bridges and outdoor full-size iron bridges [24]. Shao et al. employed MOPSO to optimize gas metal arc welding parameters for T-joints and validated the results through finite element simulations [25]. Omkar applied vector-evaluated PSO (VEPSO) to reduce the weight and total cost of composite structures under specified strength constraints [26]. Perez and Behdinan developed a two-stage truss optimization design method using an improved PSO algorithm, achieving lower structural weight under given load requirements [27]. Mokarram and Banan proposed a PSO-based multi-objective structural optimization method applicable to both discrete and continuous design variables, significantly improving optimization efficiency [28]. Goodarzimehr et al. combined PSO with genetic algorithms (GAs) to propose a spatial structure optimization algorithm, which demonstrated strong performance in truss structure optimization [29]. These studies indicate that PSO-based algorithms exhibit strong transferability in engineering applications and can achieve favorable optimization results.

Optimization and modeling methods have also been applied to electromagnetic and electrodynamic vibration-related systems. Chiu et al. optimized the design parameters of an electromagnetic vibration-based energy harvester and showed that coil, magnet, damping, excitation frequency, and geometric constraints jointly affect the generated electrical power [30]. Fickenwirth investigated electrodynamic shaker capability estimation through experimental dynamic substructuring, demonstrating the importance

of shaker physics, frequency-response characteristics, and dynamic coupling in vibration testing [31]. Wang et al. applied PSO together with surrogate models to reduce electromagnetic vibration in a permanent magnet synchronous motor, and verified the optimized design using finite element simulation and experimental measurement [32]. Jiang et al. analyzed a moving-magnet linear motor for a linear compressor and showed that motor force, magnetic spring effect, and resonant frequency are important for the overall performance of linear electromagnetic machines [33]. These studies provide valuable references for electromagnetic system modeling and optimization. However, their optimization or evaluation criteria mainly concern electrical power, force capability, vibration response, resonant frequency, or electromagnetic performance. For the electrodynamic vibrator, thermal characteristics can also constrain dynamic performance, especially the reliability of long-term operation. Therefore, the present study focuses on the thermal pre-design of the armature coil of a high-propulsive-force electrodynamic vibrator, where Joule heat generation and cooling-water-channel geometry are treated as the main competing design objectives.

For high-propulsive-force electrodynamic vibrators, armature-coil heat generation and internal temperature rise are key factors that limit long-term operating reliability. The present study does not aim to develop a new MOPSO algorithm, but to establish a pre-design-stage thermal optimization framework for armature-coil parameter selection under a prescribed rated propulsive-force requirement. In this framework, the required driving current is estimated from the force condition, and two physically related but competing objectives are formulated: Joule heat generation in the armature coil and the geometric balance between the cooling-water channel and conductive cross-section. Winding configuration, coil cross-sectional dimensions, number of turns, and geometric constraints are then treated in a unified MOPSO-based procedure to obtain a Pareto-optimal solution set rather than a single empirical design. Finite element thermal simulations are further used as numerical verification to evaluate the temperature distribution of representative designs.

The structure of this manuscript is organized as follows: Section 2 presents the structure of the electrodynamic vibrator and the optimization objectives considered in the design. Section 3 briefly introduces multi-objective optimization problems and the MOPSO algorithm. Section 4 describes the PSO-based parameter optimization procedure for the armature coil design of the electrodynamic vibrator. Section 5 presents a rated propulsive force optimization case study of an electrodynamic vibrator and uses finite element analysis to compare the armature coil temperature before and after optimization, thereby verifying the effectiveness of the proposed approach. Section 6 presents the discussion and conclusions.

2. Structure of Electrodynamic Vibrator and Optimization Objective

To establish the objective functions required in the optimization algorithm for the design of electrodynamic vibrators, the basic structure of the electrodynamic vibrator is first introduced. The configuration considered in this study is an electrodynamic vibrator with a dual excitation coil structure [2], as shown in Figure 2. Two excitation coils are arranged to generate a strong magnetic field in the air gap, while the armature coil is placed in the effective magnetic-field region. The alternating current in the armature coil interacts with the magnetic field and produces axial electromagnetic force, which is transmitted to the shaker table.

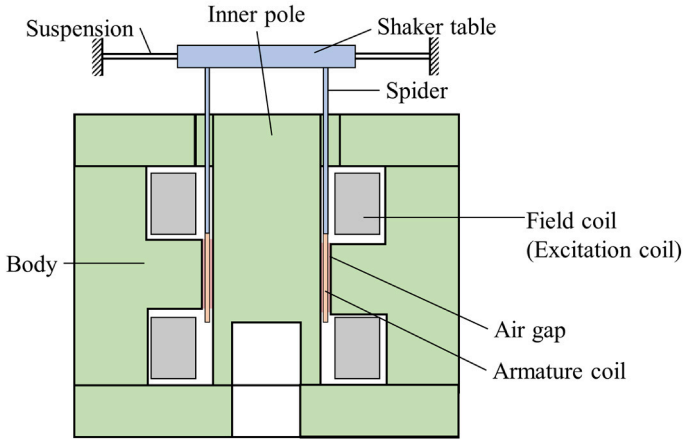


Figure 2. Schematic diagram of the electrodynamic vibrator structure.

The excitation coils of the electrodynamic vibrator generate an approximately uniform magnetic field within the air gap. When an electric current flows through the armature coil, an electromagnetic force is produced in the magnetic field, which constitutes the force acting on the armature coil connected to the shaker table. The electromagnetic force acting on a current-carrying conductor can be obtained from the Lorentz force. Accordingly, the propulsive force F_p of the electrodynamic vibrator can be expressed as

$$\boldsymbol{F_p} = I_a \int_L d\boldsymbol{I} \times \boldsymbol{B}, \tag{1}$$

where F_p denotes the propulsive force of the vibrator and I_a is the current in the armature coil. In the active region of the armature coil, the magnetic field in the air gap is approximately uniform and the current direction is nearly perpendicular to the useful magnetic-field component. Therefore, the axial propulsive force can be approximated as

$$F_p = I_a \int_{L_{a_{eff}}} B_e \, dl \approx B_e I_a L_{a_{eff}}, \tag{2}$$

where B_e is the magnetic field intensity generated by the excitation coils in the air gap. $L_{a_{eff}}$ represents the effective length of the armature coil, which is the length of coil located within the air gap. This simplified expression is used for pre-design-stage current estimation. With given F_p in the pre-design stage, I_a could be obtained with given L_{aeff}:

$$I_a = \frac{F_p}{B_e L_{aeff}}. \tag{3}$$

The effective length $L_{a_{eff}}$ of the armature coil depends on the winding configuration, as illustrated in Figure 3. The cross-section of the armature coil is shown in Figure 3c. In Figure 3, the orange regions represent the conductor of the armature coil which carries current, while the blue regions in the center denote the cooling water channel. The design parameters a, b and t determine the cross-sectional areas of the conductive region and the cooling water channel, thereby influencing the electrical resistance, heat generation, and heat dissipation efficiency. These factors jointly affect the internal temperature of the electrodynamic vibrator during operation. Consequently, the optimization design in this study adopts two objectives: the ratio between the cooling water cross-sectional area and the conductive cross-sectional area, and the total heat generation of the armature coil.

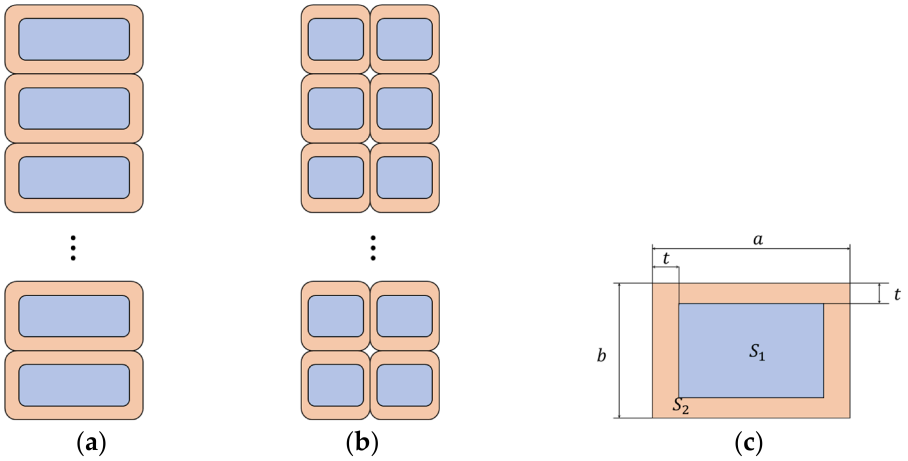


Figure 3. Armature coil winding configurations: (**a**) single-layer, (**b**) double-layer. (**c**) Schematic diagram of the armature coil cross-section.

Under identical propulsive force requirements, a single-layer winding configuration requires larger current due to its shorter effective coil length, which increases the heat generation in the armature coil. In contrast, a double-layer winding configuration reduces the effective conductor cross-sectional area, resulting in higher electrical resistance and a smaller cooling water channel, which also leads to increased heat generation. To quantitatively evaluate the performance of different winding configurations and parameter selections, coil heat generation is adopted as an objective for evaluating coil design quality.

The design parameters of the armature coil include the number of turns (number of layers), winding configuration (single-layer or double-layer), and the cross-sectional area of the conductive region. Based on these parameters, the thermal power W_a generated by the armature coil under maximum propulsive force conditions can be calculated as

$$W_a = I_a^2 R_a, \tag{4}$$

where R_a is the electrical resistance of the armature coil. The resistance can be expressed in terms of the conductive area of the armature coil S_2 and the electrical resistivity λ (unit: Ω·m) of the coil material as

$$R_a = \frac{\lambda L_a}{S_2}. \tag{5}$$

The effective length of the armature coil $L_{a_{eff}}$ can be determined from the coil diameter d and the number of turns (or layers) N as

$$L_a = N\pi d. \tag{6}$$

The cross-sectional area of the cooling water channel S_1 and the conductive area of the armature coil S_2 can be derived from the geometric parameters a, b and t as

$$S_1 = (a - 2t)(b - 2t), \tag{7}$$

$$S_2 = ab - S_1 = 2t(a + b) - 4t^2. \tag{8}$$

The first objective is to evaluate the effect of water cooling:

$$J_1 = \left(1 - \frac{S_1}{S_2}\right)^2. \tag{9}$$

This geometric objective serves as a surrogate for a detailed heat-transfer model, in order to balance the cooling space and conductive material in a pre-design stage. The second objective is the Joule heat generation of the armature coil:

$$J_2 = W_a = I_a^2 R_a. \tag{10}$$

3. Particle Swarm Optimization Algorithm

PSO is an evolutionary algorithm inspired by the social behavior of bird flocks. Multi-objective PSO (MOPSO), an extension of PSO, introduces the concept of Pareto optimization and has been widely used in the field of multi-objective optimization. In a d-dimensional decision space, a population comprising N particles, denoted as $\boldsymbol{X} = (\boldsymbol{X}_1, \boldsymbol{X}_2, \ldots, \boldsymbol{X}_N)$, is initialized. Each particle i corresponds to a d-dimensional vector that defines its location within the search domain, thereby representing a candidate solution to the optimization problem. The MOPSO algorithm starts by generating the swarm randomly, with both the initial positions and velocities of the particles assigned in a stochastic manner. Among the configurable parameters in MOPSO is the population size, i.e., the number of particles. The optimization process is guided by two distinct objectives, as mentioned in the previous section:

$$J_1 = \left(1 - \frac{S_1}{S_2}\right)^2, \tag{11}$$

$$J_2 = W_a. \tag{12}$$

Within the MOPSO framework, each candidate solution (particle) is quantitatively assessed using the objective functions. A non-dominated solution set is maintained in an external archive, known as the repository (REP). The REP's operations are managed by two core mechanisms [34]: an archive controller and a grid system. The controller adjudicates the admission of new particles by performing a dominance check; a particle is incorporated into the REP only if it is non-dominated compared to the existing archive members. These archived, non-dominated solutions serve as leaders for the swarm [35]. Concurrently, the grid mechanism organizes the archival space into adaptive hypercubes, which are utilized to monitor and preserve the diversity of the solutions along the Pareto front.

As an iterative search methodology, MOPSO refines the swarm by progressively updating the decision variables of each particle. Throughout this process, every particle retains the best position it has personally discovered, denoted as p_b (personal best). The swarm is collectively guided by a global best position, g_b, which is selected from the non-dominated solutions in the repository (REP). To promote diversity in the Pareto front, the g_b leader is typically chosen from the least crowded hypercube within the REP using a roulette wheel selection mechanism.

During the iterative process, each particle's trajectory is determined by sequentially updating its velocity and position. The update rules are governed by the following equations:

$$v_{k,j}^{iter+1} = w v_{k,j}^{iter} + c_1 r_1 \left(pb_{k,j}^{iter} - x_{k,j}^{iter}\right) + c_2 r_2 \left(gb_j^{iter} - x_{k,j}^{iter}\right), \tag{13}$$

and

$$x_{k,j}^{iter+1} = x_{k,j}^{iter} + v_{k,j}^{iter+1}, \tag{14}$$

where $x_{k,j}^{iter}$ and $v_{k,j}^{iter}$ are the j-th component of x and v of the k-th particle at iteration $iter$. The parameters in the equations are defined as follows: w (inertia), c_1 (cognitive factor), c_2 (social factor), and r_1, r_2 (uniform random numbers in [0, 1]). These parameters balance the influence between the particle's own best solution (P_best) and the swarm's best solution (G_best). To avoid premature convergence and preserve diversity, the global leader is selected

from less crowded grid regions of the repository. When the number of non-dominated solutions exceeds the repository size, solutions in crowded grid regions are preferentially removed. This repository and grid mechanism enables the algorithm to maintain a well-distributed approximation of the Pareto front. A more detailed discussion on MOPSO is given in recent reviews of PSO and MOPSO [36,37].

The Pareto front in MOPSO comprises a spectrum of non-dominated solutions, each embodying a different compromise between the conflicting objectives. In the case of two objectives, Figure 4 shows that while one extreme solution is superior for objective 1, it is weak in objective 2, and vice versa for the opposite extreme. Solutions in the center of the front offer a middle ground, providing balanced performance without being extreme in either objective. This highlights the inherent trade-offs involved in selecting a final solution.

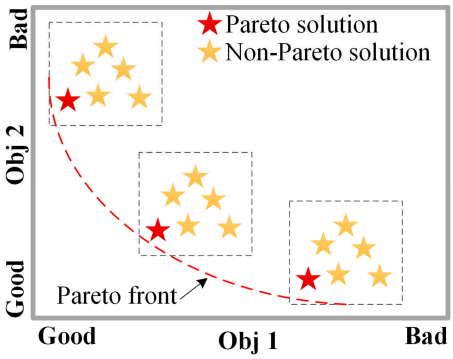


Figure 4. Pareto set of MOPSO.

4. Optimization Design Procedure for the Armature Coil of Electrodynamic Vibrator

The proposed MOPSO-based armature coil optimization design procedure is employed for the pre-design stage of an electrodynamic vibrator. The procedure can be divided into three main parts: pre-design stage (deciding the armature coil configuration), MOPSO stage (searching for potential best armature coil designs), and verification stage (selecting the best design).

In the preliminary design stage, the basic configuration of the electrodynamic vibrator is first determined, including the structural form and several fundamental geometric dimensions. At this stage, the design parameters to be optimized are identified, and their corresponding ranges and characteristics are specified. These characteristics include, for example, whether a parameter is continuous or discrete (e.g., the number of coil layers being an integer) and whether a design choice is categorical (e.g., single-layer or double-layer winding configuration of the armature coil). In addition, physical, geometric, and manufacturing constraints—such as maximum allowable dimensions, material properties, and rated propulsive force requirements—are defined. The parameters determined during the preliminary design stage are subsequently introduced into the optimization stage either as fixed values or as explicit constraints.

In the parameter optimization design stage, the optimization problem is formulated based on the design variables, constraints, and multi-objective functions established in the previous stages. Under the constraints determined during preliminary design, the multi-objective optimization algorithm is employed to search for the optimal boundary set of design parameters, namely the Pareto front. Each solution on the Pareto front represents a trade-off between competing objectives, such as minimizing armature coil heat generation and improving heat dissipation capability. During the optimization process, candidate solutions are iteratively updated according to the MOPSO strategy, and infeasible

solutions that violate predefined constraints are discarded or penalized to ensure physical realizability and engineering feasibility.

In the post-processing and verification stage, the obtained Pareto-optimal solutions were further analyzed. From the Pareto front, parameter sets that are suitable for practical manufacturing, exhibit reasonable geometric proportions, and satisfy engineering experience are selected. These selected parameter combinations are then evaluated using finite element simulations to assess thermal performance under rated operating conditions. Key indicators such as temperature distribution, peak temperature of the armature coil, and thermal gradients are examined to verify the effectiveness and robustness of the optimized design. By comparing the simulation results before and after optimization, the advantages of the proposed optimization strategy in reducing heat generation and improving thermal performance can be quantitatively demonstrated.

The complete optimization design workflow, encompassing preliminary design, multi-objective parameter optimization, and numerical verification, is summarized in the flowchart shown in Figure 5.

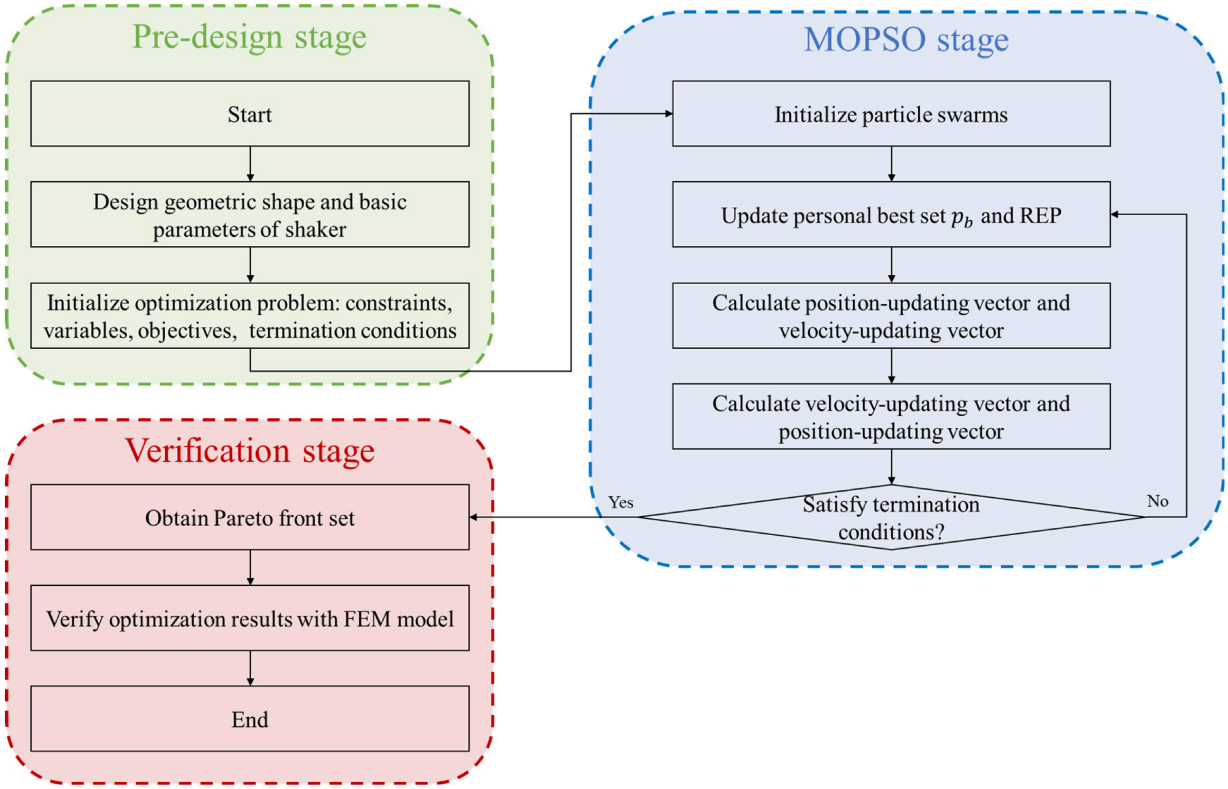


Figure 5. Design optimization procedure of electrodynamic vibrator.

In the present workflow, the dynamic requirements of the electrodynamic vibrator, such as rated force, loading-frequency range, moving-system configuration, and resonance margin, are regarded as system-level design conditions rather than optimization objectives of the armature-coil thermal design. This is because the dynamic behavior of the vibrator depends not only on the armature coil, but also on the shaker table, suspension, fixture, payload, and overall structural stiffness. Therefore, in the present pre-design-stage coil optimization, the rated propulsive force and geometric envelope are prescribed, and the optimization focuses on reducing Joule heat generation and improving cooling capability within these constraints. Dynamic performance will be considered separately in the overall vibrator system design.

5. Optimization Case Study and Finite Element Verification

Following the multi-objective parameter optimization design procedure described in Section 4, a multi-objective optimization of the armature coil is conducted for the electrodynamic vibrator under a prescribed propulsive force requirement. The optimization focuses on two thermal design objectives: reducing Joule heat generation in the armature coil and maintaining a suitable balance between the cooling-water-channel area and the conductive cross-sectional area. Prior to optimization, the armature coil assembly and vibrator structure are preliminarily designed to determine the constraints of the optimization problem.

According to the requirements of the vibrator platen, the average diameter of the armature coil is set to 1146 mm, with a total coil thickness of 38 mm. The number of coil layers considered is limited to no more than two, and for multilayer configurations, the number of turns in each layer is assumed to be equal. In addition, the total height of the armature coil is constrained to be less than 350 mm. The grid size of length parameters, including b and t, is set to be 0.5 mm. These conditions define the geometric and physical feasibility boundaries for the optimization problem. The design propulsive force F_p of the vibrator is 10^6 N. The current in the armature coil could then be obtained with Equation (3).

The numerical implementation of MOPSO is given in Table 1.

Table 1. MOPSO parameter values.

Parameter	Population Size N_p	Maximum Iteration N_{iter}	Repository Size N_{REP}	Grid Number n_{grid}	Cognitive Factor c_1	Social Factor c_2
Value	50	200	100	12	1.5	1.5

In the present implementation, the maximum iteration number was used as the main termination criterion. The convergence curves of J_1 and J_2 were then examined to confirm that the repository solutions became stable before the final iteration. The inertia weight was set as $w = 0.8$, and the cognitive and social factors were set as $c_1 = c_2 = 1.5$. The repository size was 100, and the adaptive grid number was 12. Infeasible particles violating geometric constraints, including negative cooling-channel dimensions, excessive total coil height, and nonmanufacturable discrete dimensions, were rejected during the objective-function evaluation. The geometric parameters b and t are discretized using a 0.5 mm grid to reflect manufacturability.

By applying the multi-objective optimization procedure described previously, a set of Pareto-optimal solutions satisfying the optimization objectives was obtained, as shown in Figure 6.

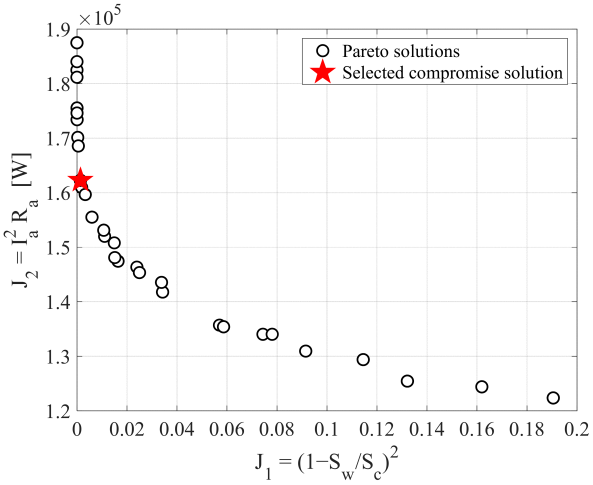


Figure 6. Pareto solutions of armature coil optimization.

The convergence history of the two objective functions is shown in Figure 7.

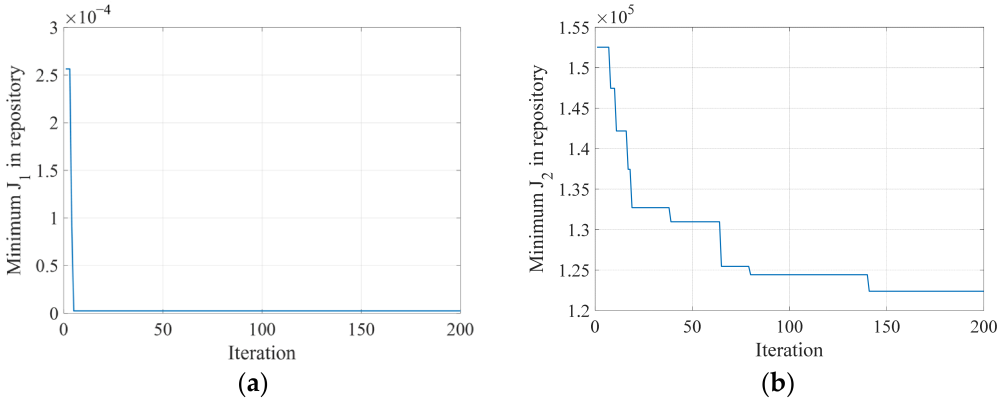


Figure 7. Convergence history curve of (**a**) J_1 (**b**) J_2.

Figure 7 shows that both J_1 and J_2 converge within 200 iterations. J_1 converges more rapidly than J_2. Figure 6 shows the conflict between the two objectives J_1 and J_2. The distribution of the nondominated solutions clearly indicates a trade-off between the two objectives. A decrease in J_1, corresponding to a better balance between the cooling-water channel area and the conductive cross-section, is accompanied by an increase in J_2. Conversely, reducing Joule heat requires a larger deviation of the sectional balance. This confirms that the armature-coil design problem is inherently multi-objective and that a single-objective optimization strategy may lead to a biased design. A preliminary sensitivity analysis was also performed by varying the population size, inertia weight, learning factors, and grid number. The obtained Pareto fronts showed similar distributions within the tested parameter ranges, indicating that the main trade-off trend between J_1 and J_2 was not strongly dependent on a single MOPSO parameter setting.

Among these Pareto solutions, a two-layer coil configuration is selected as a representative optimal design with FEM verification. Since cooling efficiency is of great importance in long-time operation of an electrodynamic vibrator, the compromise solution x^* is selected for $J_1 \leq 0.04$ with $x^* = \underset{x \in \mathcal{P}}{\operatorname{argmin}} J_2(x)$, as shown in Figure 6. The corresponding design parameters are listed in Table 2.

Table 2. Optimized design parameters of the armature coil.

Parameter	a (mm)	b (mm)	t (mm)	S_1/S_2	Effective Length L_{aeff} (m)
Value	19	32	3.5	0.97	70

To verify the effectiveness of the proposed multi-objective optimization method, finite element simulations are performed to evaluate the temperature distribution of the armature coil under the maximum propulsive force condition. In the simulations, the electrodynamic vibrator is simplified as an axisymmetric model, which significantly reduces computational cost while preserving the dominant thermal and electromagnetic characteristics of the system. Several representative parameter sets are selected as comparison cases, including both single-layer and double-layer coil configurations, as summarized in Table 3. Case 3 is the obtained optimal parameter set.

Table 3. Comparison of armature coil design parameters for finite element simulations.

Parameter Set Case No.	1	2	3 (Optimal)	4	5	6
Coil layers	Single	Double	Double	Double	Double	Double
a (mm)	38	19	19	19	19	19
b (mm)	24.5	20	32	40	32	32
t (mm)	3.5	3.5	3.5	3.5	2.5	4.5
S_1 (mm^2)	542.5	156	300	396	378	230
S_2 (mm^2)	388.5	224	308	364	230	378
S_1/S_2	1.4	0.7	0.97	1.09	1.64	0.61
Number of turns	13	16	10	8	10	10
L_{eff} (m)	48	118	70	59	70	70

The finite element thermal simulations were performed using COMSOL Multiphysics (Version 6.1). To reduce the computational cost while retaining the dominant radial–axial heat-transfer characteristics of the vibrator, an axisymmetric model was adopted. This simplification is reasonable because the excitation coils, armature coil, magnetic circuit, and cooling channel are approximately annular in the main working region. The Joule heat generated in the armature coil was applied as the internal heat source according to the calculated electrical power under the rated propulsive-force condition. The cooling of the armature coil was modeled by prescribing a water-flow inlet boundary condition. The total cooling-water flow rate of the moving coil was approximately 110 L/min. The inlet velocity was calculated from the cooling-channel cross-sectional area as $v_{in} = \frac{Q}{S_{1total}}$, where Q is the volume flow rate and S_{1total} is the total cross-sectional area of the cooling-water channel. The inlet water temperature was set to 25 °C. The material of the coils is copper, and that of the vibrator body is steel. The heat source is the Joule heat under $F_p = 10^6$ N. A mesh-independence check was also performed by comparing the peak armature-coil temperature under different mesh densities. The variation in peak temperature between the adopted mesh and a finer mesh is less than 1%, indicating that the adopted mesh was sufficient for the comparative thermal analysis.

It should be noted that the axisymmetric model neglects local three-dimensional effects, such as coil lead-out regions, inlet and outlet details of the cooling channel, circumferential non-uniformity of water flow, and manufacturing asymmetry. Therefore, the present FEM model is used for comparative numerical verification at the pre-design stage, whereas a full three-dimensional coupled electromagnetic–thermal–fluid model will be needed for final engineering validation.

The temperature fields of the armature coil under maximum propulsive force conditions for the above parameter sets are compared, as shown in Figure 8.

By comparing the results of the single-layer and double-layer armature coil designs (Figure 8a,c), it can be observed that the double-layer configuration significantly increases the effective coil length, enabling the required design propulsive force to be achieved with lower driving current. As a result, both the peak temperature and the overall temperature level of the double-layer coil are substantially lower than those of the single-layer configuration.

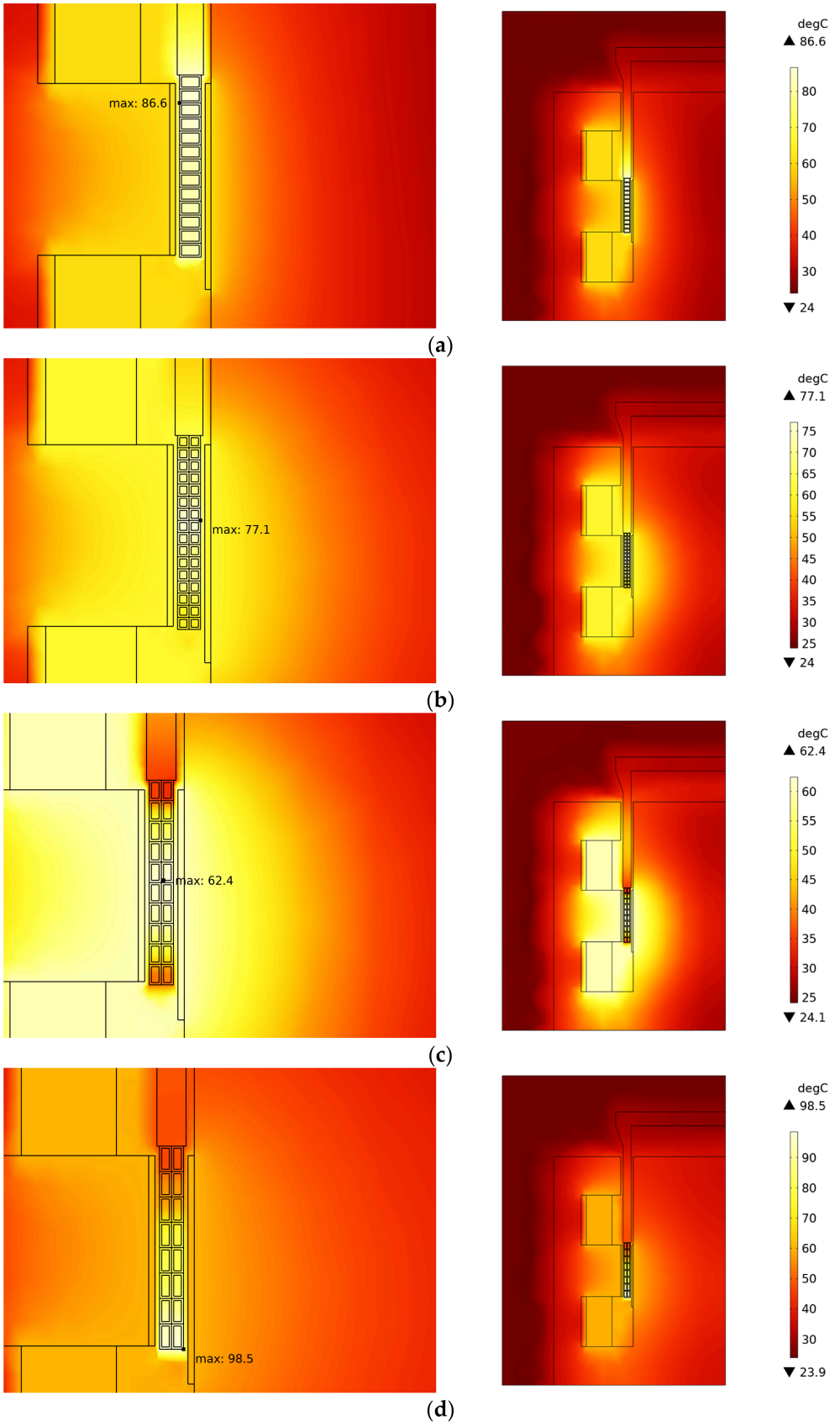


Figure 8. *Cont.*

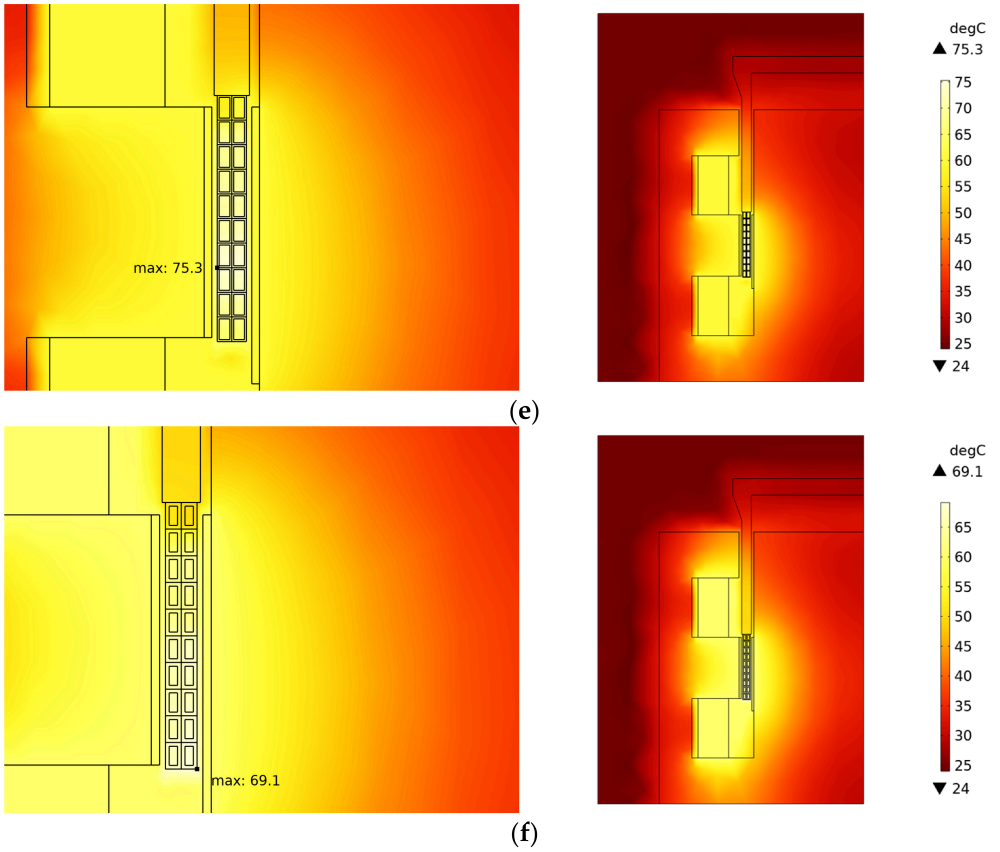


Figure 8. Temperature field inside electrodynamic vibrator for different parameter cases: (**a**) Case 1, (**b**) Case 2, (**c**) Case 3, (**d**) Case 4, (**e**) Case 5 and (**f**) Case 6.

Among the double-layer coil designs with different geometric parameters, Parameter Set 3 (Figure 8c), which corresponds to the solution obtained from the multi-objective optimization, exhibits a moderate effective length. Although the driving current under rated propulsive force is not the minimum among all design cases, the optimized balance between cooling water channel area and electrical heat generation enables Parameter Set 3 to achieve the lowest maximum coil temperature and the lowest overall temperature distribution among all of the simulated cases.

A comparison of Parameter Sets 2 (Figure 8b), 3 (Figure 8c), and 4 (Figure 8d) shows that, with the coil thickness t held constant, variations in the coil cross-sectional dimensions significantly affect the cooling water channel area. This, in turn, alters the driving current required to achieve rated propulsive force and ultimately influences the coil temperature compared to the optimal design (Parameter Set 3).

Parameter Set 2 reduces the height of each coil layer, thereby increasing the effective coil length and reducing the required current at rated propulsive force. However, the accompanying reduction in the cooling water channel area weakens heat dissipation, resulting in a higher coil temperature than that of Parameter Set 3.

Similarly, for Parameter Set 4, although the enlarged cooling water channel area enhances cooling capability, the increased height of each coil layer reduces the effective coil length and increases the required current at the rated propulsive force. This leads to higher electrical heat generation, causing the overall coil temperature to exceed that of Parameter Set 3.

Compared with Parameter Set 3, Parameter set 5 (Figure 8e) and set 6 (Figure 8f) vary the coil thickness while maintaining the overall coil cross-sectional dimensions. Although Case 5 increases the cooling water channel area, the reduction in conductive cross-sectional

area raises electrical resistance and heat generation, resulting in a higher coil temperature than that of Parameter Set 3. Similarly, for Parameter Set 6, smaller cooling water channel area reduces the cooling efficiency. The reduction in heat release brought about by the decrease in resistance cannot compensate for the reduction in cooling efficiency. As a result, the temperatures of Case 5 and Case 6 are both higher than the optimal case.

The peak temperature of each case and the reduction in Case 3 are given in Table 4.

Table 4. Peak temperature comparison of different cases.

Case	Peak Temperature (°C)	Relative Reduction in Case 3
1	86.6	27.9%
2	77.1	19.1%
3	62.4	-
4	98.5	36.6%
5	75.3	17.1%
6	69.1	9.7%

The results in Table 4 show that the selected Pareto-optimal design does not simply maximize the cooling-channel area or minimize the current. Instead, it provides a compromise between conductor area, cooling-channel area, effective length, and electrical resistance.

From an engineering perspective, the optimized variables correspond to directly manufacturable coil parameters, including winding configuration, conductor dimensions, wall thickness, and number of turns. The 0.5 mm discretization of b and t reflects the selection of practical dimensions during preliminary design. The proposed optimization procedure can reduce repeated FEM trial-and-error calculations by screening feasible coil geometries analytically before numerical verification. For larger or smaller electrodynamic vibrators, the same framework can be applied by updating the prescribed propulsive force, average coil diameter, magnetic flux density, allowable coil height, and cooling-flow conditions.

Through the comparative analysis of these parameter cases, the reliability and effectiveness of the proposed multi-objective optimization design method are verified. The results demonstrate that the optimization strategy successfully balances competing objectives: cooling performance and electrical heat generation. The proposed multi-objective design procedure leads to a design with superior thermal performance under high-propulsive-force operating conditions.

6. Conclusions and Discussion

This study investigates the parameter optimization of directly coupled electrodynamic vibrators under high propulsive force requirements, focusing on the trade-off between electrical heat generation and water-cooling performance in armature coil design. Based on theoretical analysis, quantitative objective functions are established to characterize circuit heat dissipation and cooling effectiveness, and a MOPSO framework is developed to solve the resulting optimization problem. By estimating the driving current required for a given propulsive force and evaluating coil resistance using material properties, the electrical heat generation of the armature coil is quantitatively modeled. In parallel, the ratio between the conductive cross-sectional area and the cooling water channel area is introduced as an indicator of cooling performance. These objectives are jointly optimized to balance competing thermal and electromagnetic requirements. Finite element simulations under identical propulsive force conditions demonstrate that the optimized coil parameters yield

the lowest peak and overall temperatures among the evaluated designs, verifying the effectiveness of the proposed optimization approach. The method significantly reduces reliance on exhaustive finite element analyses and improves design efficiency. Moreover, the proposed framework can be extended to other vibrator parameter design problems involving conflicting objectives.

The present study is limited by the simplified magnetic field assumption, steady-state thermal analysis, and numerical verification without experimental temperature measurements. In addition, this work focuses on armature-coil thermal pre-design under prescribed system-level requirements; dynamic indicators such as moving mass, loading-frequency range, and resonance margin are considered separately in the overall vibrator system design. Future work will incorporate experimental validation, transient electromagnetic–thermal–fluid coupling, and system-level dynamic criteria to further improve the applicability of the proposed framework.

Author Contributions: Conceptualization, X.F.; methodology, X.F.; software, X.F., J.S. and Z.L.; validation, X.F., M.Z., J.S. and Z.L.; formal analysis, X.F.; investigation, X.F.; resources, X.F. and M.Z.; data curation, X.F.; writing—original draft preparation, X.F.; writing—review and editing, X.F., M.Z., J.S. and Z.L.; visualization, X.F.; supervision, M.Z.; project administration, X.F. and M.Z.; funding acquisition, X.F. All authors have read and agreed to the published version of the manuscript.

Funding: This research was funded by the National Key Basic Research and Development Program, grant number 2023YFF0713400; Suzhou Science and Technology Plan Project-Key Industrial Technology Innovation and Key R&D Industrialization Project, grant number SGC2020102.

Data Availability Statement: The original contributions presented in this study are included in the article. Further inquiries should be directed to the corresponding author.

Conflicts of Interest: Author Xiaohong Fu was employed by the company Dongling Technologies Co., Ltd. The remaining authors declare that the research was conducted in the absence of any commercial or financial relationships that could be construed as potential conflicts of interest.

Abbreviations

The following abbreviations are used in this manuscript:

PSO	Particle Swarm Optimization
MOPSO	Multi-Objective PSO
VEPSO	Vector-Evaluated PSO
GA	Genetic Algorithms
REP	Repository

References

1. Lang, G.F. Electrodynamic shaker fundamentals. *Sound Vib.* **1997**, *31*, 14–23.
2. Wang, P.; Deng, H.; Liu, Y.; Wang, Y.M.; Zhang, Y.; Tang, Z.D. Method for increasing the speed of an electrodynamic shaker for vibration test of rolling stock equipment. *J. Vib. Control* **2023**, *29*, 225–235.
3. Nali, P.; Bettacchioli, A.; Landi, G.; Gnoffo, M. A virtual shaker testing experience: Modeling, computational methodology and preliminary results. *Adv. Aircr. Spacecr. Sci.* **2018**, *5*, 251–258.
4. Zhang, W.; Wang, X.; Li, H.; Zhou, J.; Luo, Z.; Meng, G. Vibration measurement from an adaptive phase-based motion estimation using parameter optimised log-Gabor filter. *Measurement* **2024**, *224*, 113812. [CrossRef]
5. Zhang, W.; Li, H.; Wang, J.; Hong, Y.; Meng, G. Full-field phase-based vibration measurement and visualisation using many knowledge transfer-assisted optimal log-Gabor filters. *Mech. Syst. Signal Process* **2025**, *225*, 112256. [CrossRef]
6. Darie, S.I.; Colosi, T.; Vadan, I.; Balan, H. Computational aspects of electrodynamic vibrators. In Proceedings of the Mediterranean Electrotechnical Conference (MELECON'94), Antalya, Turkey, 12–14 April 1994.
7. Yang, C.; Ye, W.; Li, Q. Review of the performance optimization of parallel manipulators. *Mech. Mach. Theory* **2022**, *170*, 104725. [CrossRef]

8. Schmit, L.A. Structural design by systematic synthesis. In Proceedings of the Second National Conference on Electronic Computation, Pittsburgh, PA, USA, 8–9 September 1960.
9. Jain, N.K.; Jain, V.K.; Deb, K. Optimization of process parameters of mechanical type advanced machining processes using genetic algorithms. *Int. J. Mach. Tools Manuf.* **2007**, *47*, 900–919. [CrossRef]
10. Xu, L.; Li, Q.; Zhang, N.; Chen, Q. Mobility, kinematic analysis, and dimensional optimization of new three-degrees-of-freedom parallel manipulator with actuation redundancy. *J. Mech. Robot.* **2017**, *9*, 041008. [CrossRef]
11. Khan, W.A.; Angeles, J. The kinetostatic optimization of robotic manipulators: The inverse and the direct problems. *J. Mech. Des.* **2007**, *128*, 168–178. [CrossRef]
12. Qiu, L.; He, Y.; Li, Y.; Yu, Y. Design and parameter optimization of a biomimetic jellyfish origami mechanism (BJOM) based on waterbomb tessellations. *Mech. Mach. Theory* **2023**, *184*, 105291. [CrossRef]
13. Zhakatayev, A.; Avazov, N.; Najjar, H.; Rogovchenko, Y.; Pätzold, M. Blind parameter identification of implicit differential equations using the collocation discretization and homotopy optimization methods. *Mech. Mach. Theory* **2024**, *200*, 105715. [CrossRef]
14. Sangalli, L.; Oyanguren, A.; Izquierdo, M.; Larrañaga, J.; Ulacia, I. Numerical study on the effectiveness of the optimization of the load distribution in ball screw actuators. *Mech. Mach. Theory* **2024**, *203*, 105781. [CrossRef]
15. Zhang, Z.; Elbashiry, M.A.E.; Chen, J.; Wei, P.; Fu, Y. Optimization of the structural parameters of the vertical trabeculae beetle elytron plate based on the mechanical and thermal insulation properties. *KSCE J. Civ. Eng.* **2020**, *24*, 3765–3774. [CrossRef]
16. Zakian, P.; Kaveh, A. Multi-objective seismic design optimization of structures: A review. *Arch. Comput. Methods Eng.* **2024**, *31*, 579–594. [CrossRef]
17. Lalwani, S.; Singhal, S.; Kumar, R.; Gupta, N. A comprehensive survey: Applications of multi-objective particle swarm optimization (MOPSO) Algorithm. *Trans. Comb.* **2013**, *2*, 39–101. [CrossRef]
18. Sharma, S.; Kumar, V. A comprehensive review on multi-objective optimization techniques: Past, present and future. *Arch. Comput. Methods Eng.* **2022**, *29*, 5605–5633. [CrossRef]
19. Eberhart, R.; Kennedy, J. A new optimizer using particle swarm theory. In Proceedings of the Sixth International Symposium on Micro Machine and Human Science (MHS'95), Nagoya, Japan, 4–6 October 1995.
20. Kennedy, J.; Eberhart, R. Particle swarm optimization (pso). In Proceedings of the IEEE International Conference on Neural Networks, Perth, WA, Australia, 27 November–1 December 1995.
21. Nanda, B.; Maity, D.; Maiti, D.K. Vibration based structural damage detection technique using particle swarm optimization with incremental swarm size. *Int. J. Aeronaut. Space Sci.* **2012**, *13*, 323–331. [CrossRef]
22. Ghodrati Amiri, G.; Zare Hosseinzadeh, A.; Seyed Razzaghi, S.A. Generalized flexibility-based model updating approach via democratic particle swarm optimization algorithm for structural damage prognosis. *Int. J. Optim. Civ. Eng.* **2015**, *5*, 445–464. [CrossRef]
23. Li, Y.; Wei, K.; Yang, W.; Wang, Q. Improving wind turbine blade based on multi-objective particle swarm optimization. *Renew. Energy* **2020**, *161*, 525–542. [CrossRef]
24. Zhang, W.; Sun, S.; Huang, J.; Hong, Y.; Li, H.; Meng, G. Multi-objective optimal log-Gabor filtering and threshold denoising for phase-based vibration measurement from noisy video. *Mech. Syst. Signal Process* **2025**, *236*, 113003. [CrossRef]
25. Shao, Q.; Xu, T.; Yoshino, T.; Song, N. Multi-objective optimization of gas metal arc welding parameters and sequences for low-carbon steel (Q345D) T-joints. *J. Iron Steel Res. Int.* **2017**, *24*, 544–555. [CrossRef]
26. Omkar, S.; Mudigere, D.; Naik, G.N.; Gopalakrishnan, S. Vector evaluated particle swarm optimization (VEPSO) for multi-objective design optimization of composite structures. *Comput. Struct.* **2008**, *86*, 1–14. [CrossRef]
27. Perez, R.E.; Behdinan, K. Particle swarm approach for structural design optimization. *Comput. Struct.* **2007**, *85*, 1579–1588. [CrossRef]
28. Mokarram, V.; Banan, M.R. A new PSO-based algorithm for multi-objective optimization with continuous and discrete design variables. *Struct. Multidiscip. Optim.* **2018**, *57*, 509–533.
29. Goodarzimehr, V.; Omidinasab, F.; Taghizadieh, N. Optimum design of space structures using hybrid particle swarm optimization and genetic algorithm. *World J. Eng.* **2023**, *20*, 591–608.
30. Chiu, M.-C.; Changm, Y.-C.; Yeh, L.-J.; Chung, C.-H. Numerical assessment of a one-mass spring-based electromagnetic energy harvester on a vibrating object. *Arch. Acoust.* **2016**, *41*, 119–131. [CrossRef]
31. Fickenwirth, P.H. Electrodynamic Shaker Capability Estimation Through Experimental Dynamic Substructuring. Master Thesis, University of California San Diego, San Diego, CA, USA, 2023.
32. Wang, Y.; Yao, L.; Shi, D.; Huang, X.; Shen, J.-X. Particle swarm optimization of electromagnetic vibration of PMSM using surrogate model. *Electr. Power Compon. Syst.* **2023**, *51*, 1963–1977. [CrossRef]
33. Jiang, H.; Liang, K.; Li, Z. Characteristics of a novel moving magnet linear motor for linear compressor. *Mech. Syst. Signal Process.* **2019**, *121*, 828–840. [CrossRef]

34. Mobin, M.; Mousavi, S.M.; Komaki, M.; Tavana, M. A hybrid desirability function approach for tuning parameters in evolutionary optimization algorithms. *Measurement* **2018**, *114*, 417–427. [CrossRef]
35. Shan, Y.; Liu, J.; Xu, Y.; Zhou, J. A combined multi-objective optimization model for degradation trend prediction of pumped storage unit. *Measurement* **2021**, *169*, 108373. [CrossRef]
36. Gad, A.G. Particle Swarm Optimization Algorithm and Its Applications: A Systematic Review. *Arch. Comput. Methods Eng.* **2022**, *29*, 2531–2561. [CrossRef]
37. Li, Z.; Han, Y.; Yang, Y. Multiobjective Particle Swarm Optimization: A Survey of the State-of-the-Art. *J. Artif. Intell. Res. Innov.* **2025**, *1*, 013–027. [CrossRef]

Disclaimer/Publisher's Note: The statements, opinions and data contained in all publications are solely those of the individual author(s) and contributor(s) and not of MDPI and/or the editor(s). MDPI and/or the editor(s) disclaim responsibility for any injury to people or property resulting from any ideas, methods, instructions or products referred to in the content.